Raman study of the substrate influence on graphene synthesis using a solid carbon source via rapid thermal annealing

Yannick Bleu, Florent Bourquard, A.-S. Loir, Vincent Barnier, Florence Garrelie, Christophe Donnet

Raman study of the substrate influence on graphene synthesis using a solid carbon source via rapid thermal annealing

Y. Bleu[1], F. Bourquard[1] A.-S. Loir[1], V. Barnier[2], F. Garrelie[1], C. Donnet[1]

(1) *Université de Lyon, Université Jean Monnet-Saint-Etienne, CNRS, Institut d'Optique Graduate School, Laboratoire Hubert Curien UMR 5516, F-42023, SAINT-ETIENNE, France*
(2) *Université de Lyon, Mines Saint-Etienne, CNRS, Laboratoire Georges Friedel UMR 5307 CNRS, F-42023 Saint-Etienne, France*

Abstract

We report the results of a comparative investigation of graphene films prepared on Si(100) and fused silica (SiO_2) combining pulsed laser deposition and rapid thermal annealing using Ni catalyst. The effect of modifying the substrate and/or growth temperature (600-1000°C) of graphene synthesis was investigated by Raman micro-spectroscopy mapping. Graphene grown on Si(100) was multilayered, and various nickel silicide phases had formed underneath, revealing dependence on the growth temperature. Films prepared on SiO_2 mainly comprised bi- and tri-layered graphene, with no traces of nickel silicide. Analysis of Raman D, G, and 2D peak intensities and positions showed that modifying the growth temperature had different effects when a Si(100) or a SiO_2 substrate is used. These findings advance our understanding of how different combinations of substrate and thermal processing parameters affect graphene synthesis from solid carbon source using nickel as a catalyst. This knowledge will enable better control of the properties of graphene film (defects, number of layers, etc.), and will have a high potential impact on the design of graphene-based devices for scientific or industrial applications.

Keywords: Graphene, pulsed laser deposition, rapid thermal annealing, nickel silicide, substrate effect.

1. Introduction

Graphene is a remarkable 2D material with a unique combination of mechanical, electronic, optical and thermal properties[1–7].These properties mean graphene could be used in many technological fields including transparent electrodes, field emitters, biosensors, batteries[8–12], to cite but a few examples. Many techniques exist for producing graphene including chemical vapor deposition, chemical reduction of graphene oxide, exfoliation, epitaxial growth on SiC or metal substrates, and physical vapor deposition methods including pulsed laser deposition (PLD)[13–30].Whatever the synthesis route chosen, many experimental factors affect the graphene nanoarchitecture and properties. However, the influence of using substrates of different natures and compositions – all other parameters being fixed – has rarely been investigated to observe their specific effects on the nature and properties of the synthetized graphene films. In the particular case of PLD, graphene growth is generally achieved using Si[31–34], SiO_2[35], SiO_2/Si[36] and Cu foil[37] substrates, with various metallic catalysts (Cu, Ni, etc.) and thermal processing techniques. Even so, it is still difficult to assess the impact of the substrate on the nature and quality of the graphene films due to changes in the PLD and thermal processing parameters from one publication to another.

A good understanding of the impact of the substrate on the nature and quality of the resulting graphene is vital for potential applications. The objective of this study was thus to synthesize graphene on two different typical substrates, crystallized silicon Si(100) and amorphous SiO_2, using the same deposition and growth process. PLD is a robust way to generate a solid carbon for graphene growth on the two different substrates. A thin Ni catalyst film is then deposited on the top surface by thermal evaporation. Finally, rapid thermal annealing (RTA) is performed in low-vacuum at temperatures between 600 and 1000°C, inducing few-layer or multilayer graphene formation as is classically reported in the literature using such carbon-nickel stacks[38]. In this way, the specific effect of the substrate on graphene-based films nanoarchitecture can be assessed, since identical deposition and heating processes are used for both substrates. The films are usually characterized by Raman micro-spectroscopy, a recognized technique for investigating the nanostructure, crystallite size, defects and number of layers in graphene materials[39–58]. Specifically, surface mapping of the Raman signal is performed to accurately assess the homogeneity of the samples at the micrometric scale. Raman spectra of carbon materials typically exhibit numerous contributions, among which three are of major significance for studying graphene: the so-called D, G and 2D peaks appearing respectively at shifts around 1350 cm^{-1}, 1580 cm^{-1} and 2700 cm^{-1}. Their shapes,

intensities, and positions provide considerable information about the graphene films, including domain sizes, defects, number of layers, and stress. The sharp G peak corresponds to the in-plane vibration mode of sp^2 hybridized carbon atoms. The D peak corresponds to the breathing of aromatic rings in the graphene lattice, and only appears in the presence of defects. The 2D peak is the result of a two-phonon lattice vibration process in graphene, observed even without any disorder or defects. The study of this last feature is probably one of the most important in characterizing the graphene-like quality of a film. The 2D on G peak intensity ratio (I_{2D}/I_G), the full width at half the maximum 2D peak (FWHM(2D)) and, to a lesser extent, the position of the 2D peak, make it possible to determine the number of layers (within 1-5) of few-layer graphene with a relatively good degree of accuracy. Given the huge amount of scientific synthesis and use of graphene, and to discuss the quality of samples produced for this study, we reviewed 50 references in the literature (see also **Supplementary S0**). Our focus was on associating I_{2D}/I_G and FWHM(2D) data with the number of layers in few-layer graphene, for the purpose of quantification. The resulting correlations are listed in **Table 1**. When the I_{2D}/I_G ratio is below 0.6, it is generally accepted that the graphene film contains more than 4 layers, with a near-certainty of more than 5 layers when I_{2D}/I_G is below 0.4. Additionally, the 2D peak position upshifts to 50 cm^{-1} when the number of layers increases from 1 to 5. For more than 4-5 layers, the FWHM(2D) cannot be used to quantify the number of layers, and the 2D signature becomes similar to that of graphite.

	I_{2D}/I_G	**FWHM(2D)**
Monolayer	> 1.3	24 - 50
Bilayer	0.7 – 2.2	38 - 65
Trilayer	0.6 – 0.7	55 - 85
4-5 Layers	0.4 – 0.6	//
Multilayers (5-10)	< 0.4	//

Table 1: Summary of I_{2D}/I_G ratio and FWHM(2D) for different graphene layers, based on 50 references (see **Supplementary S0**).

Studying the D peak is a good way to evaluate the defective nature of a graphene sample structure. Its intensity, compared to that of the G peak, can be used to investigate the quality of graphene. By studying the D to G peak intensity ratio (I_D/I_G), the crystallite size in the graphene material can be estimated using the Tuinstra-Koenig relation:

$$L_a\,(nm) = (2{,}4 \times 10^{-10})\lambda^4 \left(\frac{I_D}{I_G}\right)^{-1}$$ [59]

where λ is the laser wavelength in nanometers, and L_a is the average size of the crystallites.

This literature survey is used in section 4 to discuss the Raman results described in section 3 characterizing the graphene films obtained with various RTA parameters on both Si(100) and SiO_2 substrates.

2. Experimental

2.1. Sample preparation

The steps used to prepare the samples are shown in **Fig. 1**. First, the Si(100) and SiO_2 substrates were cleaned ultrasonically (successively in acetone, ethanol and deionized water baths). Second, amorphous carbon (a-C) was deposited by PLD in a vacuum at a base pressure of 10^{-4} Pa. The PLD targets were high purity (99.9995%) micro-crystalline graphite disks. Ablation was performed using an excimer KrF laser (248 nm wavelength, 20 ns pulse duration, 10 Hz repetition rate) at room temperature, focused with a 50 cm lens producing a 2.2 mm^2 semi-Gaussian elliptic spot. This gives an average energy density (fluence) of the laser beam at 4.5 J/cm^2. The ablation time was adjusted to keep an amorphous (a-C) film thickness of 10 nm, deposition speed having been estimated at 10 nm/min by profilometry. The substrates were mounted on a sample holder placed at a distance of 40 mm from the graphite target. A 60 nm thick nickel film was subsequently deposited by thermal evaporation on the top of the a-C/Si or a-C/SiO_2 substrate in a vacuum chamber pumped at a base pressure of 10^{-4} Pa. High purity (99.99%) Ni was heated in a tungsten nacelle and evaporated towards the substrates. The last step was rapid thermal annealing. To this end, the Ni/a-C/Si or Ni/a-C/SiO_2 samples were placed in a SiC susceptor in an RTA oven pumped at 5 Pa. The heating rate, controlled by PID, was set at 15°C/s as measured by a pyrometer located on the back of the susceptor. Cooling from high temperature was set at a maximum of 1°C/s or natural cooling (whichever is slower). Different maximum temperatures ranging from 600 to 1000°C, are reached and held for 10 minutes. **Table 2** lists the resulting samples with their label and synthesis conditions.

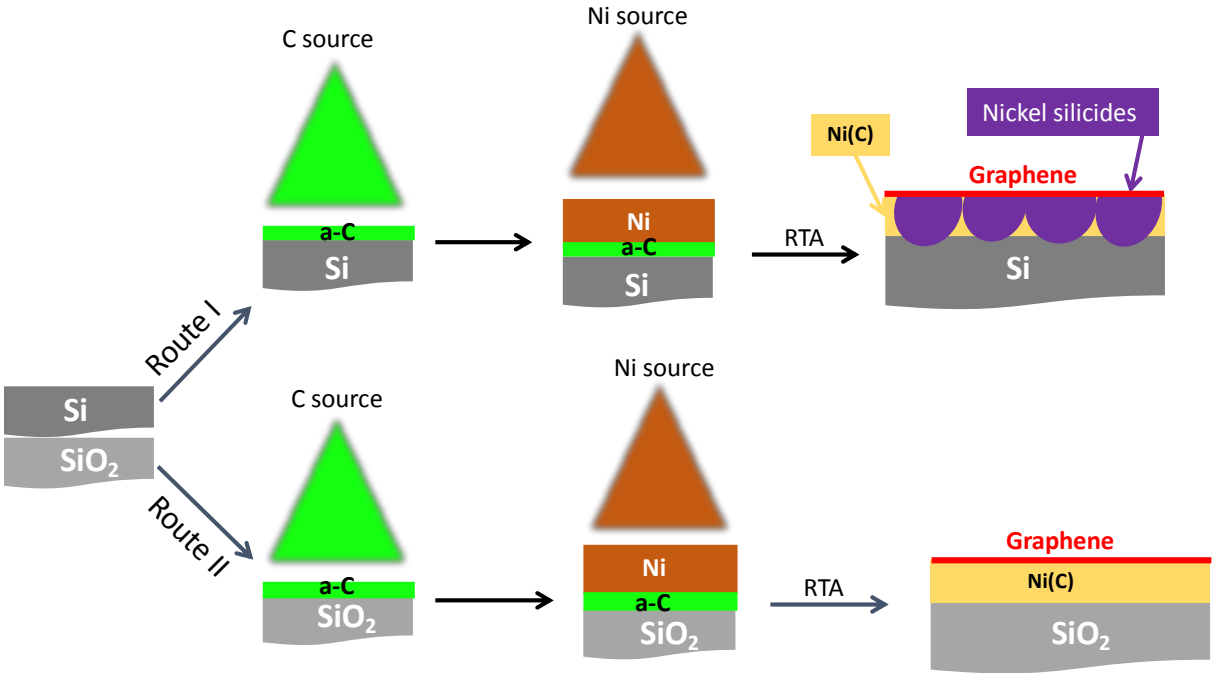

Fig. 1: Synthesis route of graphene films obtained by combining pulsed laser deposition and rapid thermal annealing on both Si(100) and SiO_2 substrates. The formation of nickel silicides with the Si(100) substrate is detailed in the "results" section.

2.2. Sample characterization

Raman spectroscopy is performed using an Aramis Jobin Yvon spectrometer. The excitation wavelength is 442 nm (He-Cd source) for graphene spectra and 633 nm (He-Ne source) for nickel silicide spectra, with a spectral resolution around 2 cm^{-1}. The excitation laser beam is focused with a 100x objective, consistent with a laser spot with a diameter < 1 µm for both wavelengths, allowing for submicrometric spatial resolution when performing Raman mapping. The laser power was kept below 3 mW to avoid damaging the film surface. Rectangular mapping was performed on all samples at 442 nm excitation wavelength. The probed surface was a 20 × 20 $µm^2$ square, with a 1 µm spatial sampling. This means that over 400 Raman spectra were collected for each sample.

A custom-made algorithm relying on the SciPy python library was then used to extract relevant information on the Raman peaks: intensity, width, position, etc. Most peaks were fitted with Lorentzian functions, except for the G peak which was fitted with a Breit-Wigner-Fano function accounting for its asymmetry compared to a classical Lorentzian profile[60]. Later, when computing intensity ratios, we will be referring, as is usually the case in the literature, to peak height (intensity maximum) as opposed to peak area. All peak properties

discussed later (FWHM, intensity maximum, positions, etc.) were extracted from the properties of the Lorentzian profiles.

	Graphene precursor & substrate	RTA temperature	Sample label
Graphene on Si(100)	Ni(60 nm)/a-C(10 nm)/Si(100)	**1000°C**	G-Si-1000
	Ni(60 nm)/a-C(10 nm)/Si(100)	**900°C**	G-Si-900
	Ni(60 nm)/a-C(10 nm)/Si(100)	**800°C**	G-Si-800
	Ni(60 nm)/a-C(10 nm)/Si(100)	**700°C**	G-Si-700
	Ni(60 nm)/a-C(10 nm)/Si(100)	**600°C**	G-Si-600
Graphene on SiO_2	Ni(60 nm)/a-C(10 nm)/SiO_2	**1000°C**	G-SiO_2-1000
	Ni(60 nm)/a-C(10 nm)/SiO_2	**900°C**	G-SiO_2-900
	Ni(60 nm)/a-C(10 nm)/SiO_2	**800°C**	G-SiO_2-800
	Ni(60 nm)/a-C(10 nm)/SiO_2	**700°C**	G-SiO_2-700
	Ni(60 nm)/a-C(10 nm)/SiO_2	**600°C**	G-SiO_2-600

Table 2: The samples and their growth conditions. RTA annealing was performed in a low vacuum at 5 Pa for 600 s, preceded by a +15°C/s heating ramp and followed by cooling limited to -1°C/s.

3. Results

3.1. Substrate effects depending on the annealing temperature

Raman mappings (20 x 20 µm², each integrating 400 Raman spectra) were performed on representative areas to highlight the similarities and differences between the graphene grown on Si(100) and SiO_2 substrates at the five growth temperatures. This made it possible to compute mappings for the following characteristics: I_D/I_G and I_{2D}/I_G intensity ratios, 2D peak FWHM, as well as D, G, and 2D peak positions. **Table 3** lists the mean values of these characteristics for each sample, averaged from each set of 400 recorded spectra. The most relevant mappings are shown and commented below, the others are provided in Supplementary information.

Fig. 2a and 2b show the Raman mapping of the I_D/I_G intensity ratio for samples grown at all temperatures, on Si and SiO_2, respectively. On the Si(100) substrate, the mean intensity ratio I_D/I_G increased with growth temperature from 0.297 to 0.468. This suggests a decrease in the mean crystallite size from 31 to 20 nm. This effect is shown in the left plot in **Fig. 2c**. On the SiO_2 substrate, the opposite behavior was observed (as shown in the right plot in **Fig. 2c**): the mean intensity ratio I_D/I_G decreased from 0.293 to 0.140 with an increase in the growth temperature. This was associated with an increase of from 31 to 65 nm in the mean crystallite size. These results suggest that graphene films grown on SiO_2 contain fewer defects and larger crystallites than graphene grown on Si(100).

	Graphene on Si(100)					Graphene on SiO_2				
RTA temperature	600°C	700°C	800°C	900°C	1000°C	600°C	700°C	800°C	900°C	1000°C
I_D/I_G	0.297	0.317	0.346	0.462	0.468	0.293	0.269	0.271	0.174	0.140
La (nm)	31	29	26	20	20	31	34	34	53	65
I_{2D}/I_G	0.438	0.477	0.403	0.427	0.342	0.412	0.420	0.489	0.706	0.721
2D position	2742	2739	2738	2745	2754	2743	2741	2737	2733	2732
2D FWHM	111	109	108	112	120	108	109	107	87	77
G position	1577	1576	1576	1584	1583	1580	1579	1576	1574	1573
D position	1367	1365	1366	1374	1373	1373	1374	1367	1361	1360

Table 3: Mean values of the Raman characteristics resulting from the 400 Raman spectra performed on representative areas of the graphene films and presented as Raman mappings in the proof and in Supplementary information.

Fig. 3a and 3b show Raman mappings of the I_{2D}/I_G intensity ratio for graphene grown at all annealing temperatures, on Si (100) and SiO_2, respectively. On the Si(100) substrate, the mean I_{2D}/I_G ratio globally decreased (albeit non-monotonically) with temperature, from 0.477 to 0.342 (as seen in Fig. 3c), whereas the mean FWHM(2D) increased slightly from 111 to 120 cm^{-1} (see **Supplementary Fig. S1**). This suggests that the number of graphene layers increases with an increasing growth temperature. The opposite behavior was observed on SiO_2 substrates, where the number of graphene layers decreased with an increase in the growth temperature from 600°C to 1000°C. As can be seen in **Fig. 3c** (right plot), the mean I_{2D}/I_G intensity ratio increased from 0.412 to 0.721 and the FWHM(2D) mean value decreased from 108 to 77 cm^{-1} (see **Supplementary S1**) with growth temperature. These results suggest that growth on SiO_2 substrates produces graphene films with fewer layers than growth on Si(100).

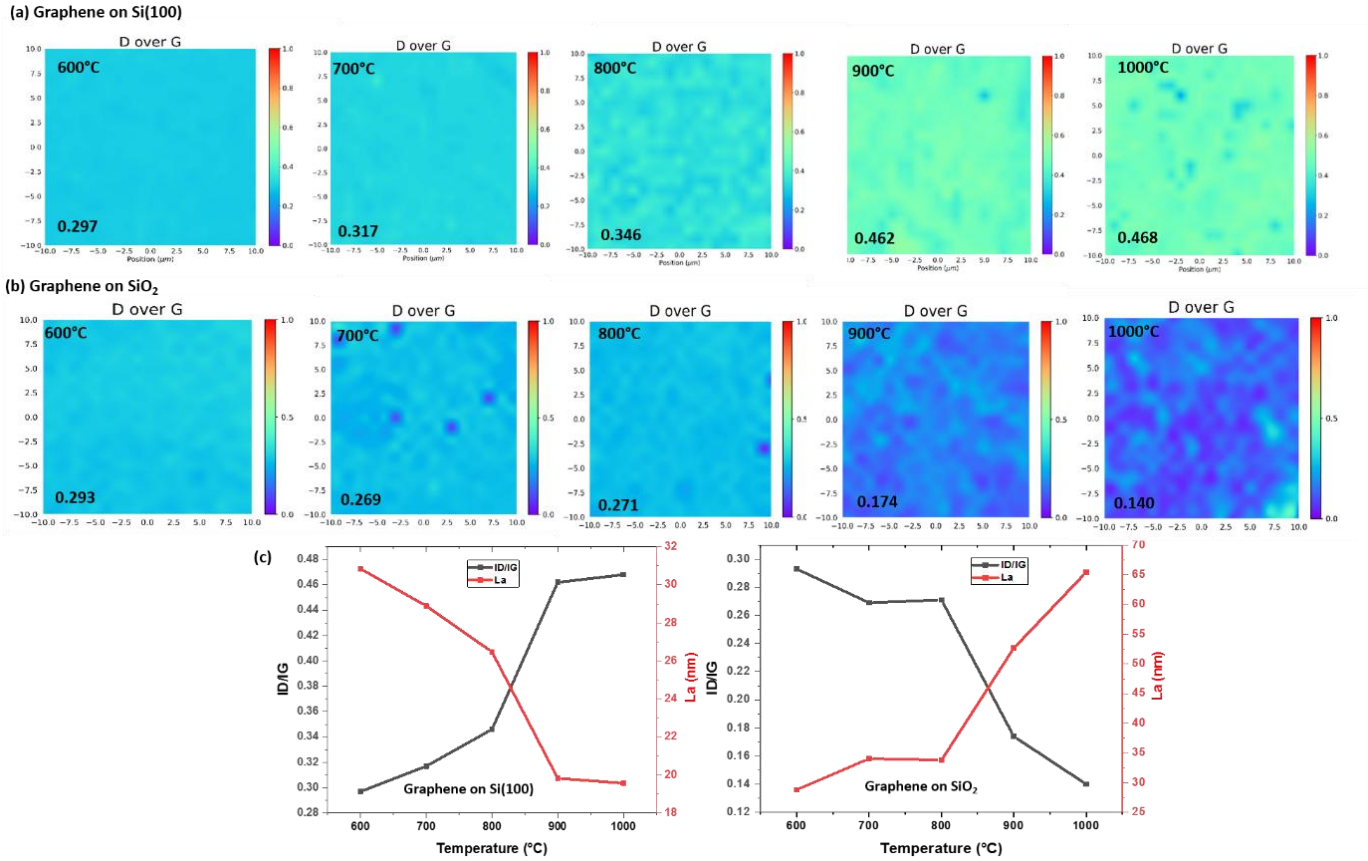

Fig. 2: (a) I_D/I_G Raman mapping of as-grown graphene at temperatures ranging from 600-1000°C on Si (100) with their mean values, (b) I_D/I_G Raman mapping of as-grown graphene at temperatures ranging from 600-1000°C on SiO_2 with their mean values, (c) Plots showing dependence on growth temperature as a function of mean I_D/I_G ratio and crystallite size (L_a): right plot, graphene on Si(100), left plot, graphene on SiO_2.

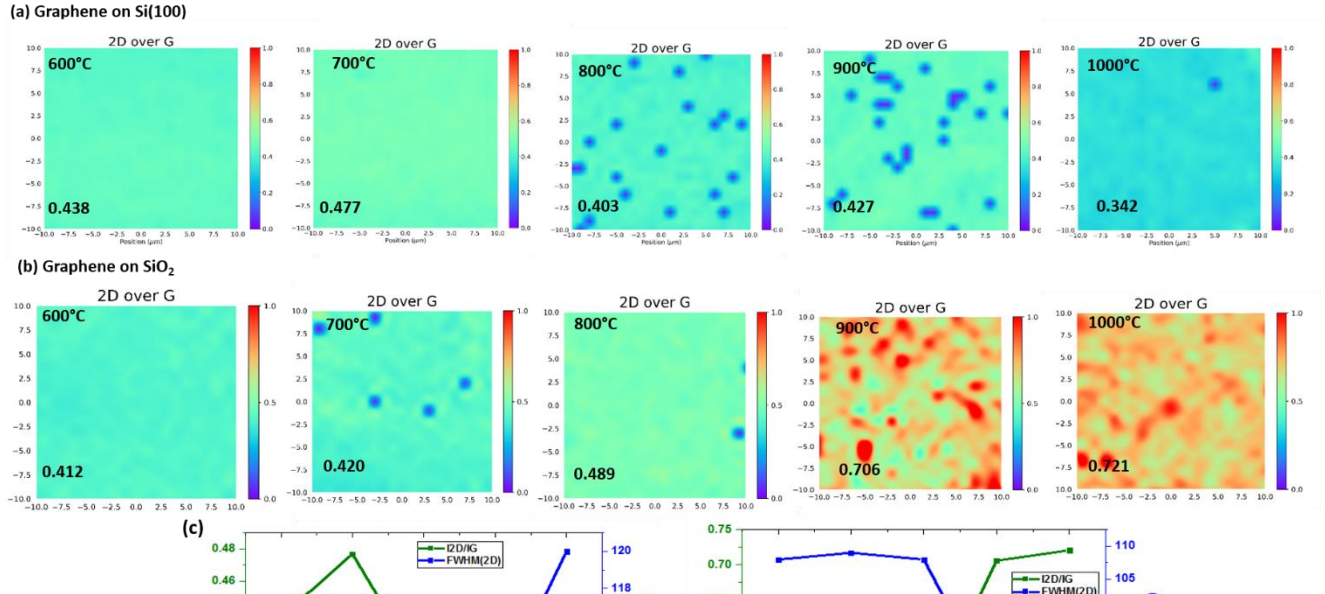

Fig. 3: (a) I_{2D}/I_G Raman mapping of as-grown graphene at temperatures ranging from 600-1000°C on Si (100) with their mean values, (b) I_{2D}/I_G Raman mapping of as-grown graphene at temperatures ranging from 600-1000°C on SiO_2 with their mean values, (c) Plot of growth temperature dependency as a function of the I_{2D}/I_G ratio and the FWHM(2D): right plot, graphene on Si (100), left plot, graphene on SiO_2.

Fig. 4 shows typical Raman spectra extracted from the mapping of each of the samples detailed in **Table 2**. The abovementioned and commented D, G, and 2D peaks are clearly visible, as are other minor peaks: D+D'' near 2450 cm^{-1}, D+G near 2950 cm^{-1} and 2D' near 3250 cm^{-1}, all already observed in some graphene films. The D + D" and 2D' peaks are, like the G and 2D peaks, common features in most graphene samples. They emerge, like the 2D peak, as a combination of two phonon modes individually associated with defects (D' and D") allowing so-called breathing of aromatic rings in carbon materials. The combination of those resonances can appear without defects as the two phonons can verify momentum conservation provided they have opposite wavevectors. In the case of the D + G peak, also sometimes labelled D + D', the excitation mechanisms are somewhat unclear but they also appear in defective graphene-like material[61,62]. The insert in **Fig.4b** shows the deconvolution of the 2D peak from a spectrum from the graphene film obtained at 1000°C on SiO_2. The 2D peak is deconvoluted into four components each with a FWHM of 28 cm^{-1}. According to Malard *et al.*[40], this is the fingerprint of bilayer graphene. It is worth mentioning that some of the spectra extracted from the mapping of this sample had a substantially larger 2D peak, which were deconvoluted into 6 components (with a FWHM of 28 cm^{-1}), which is consistent with trilayer graphene.

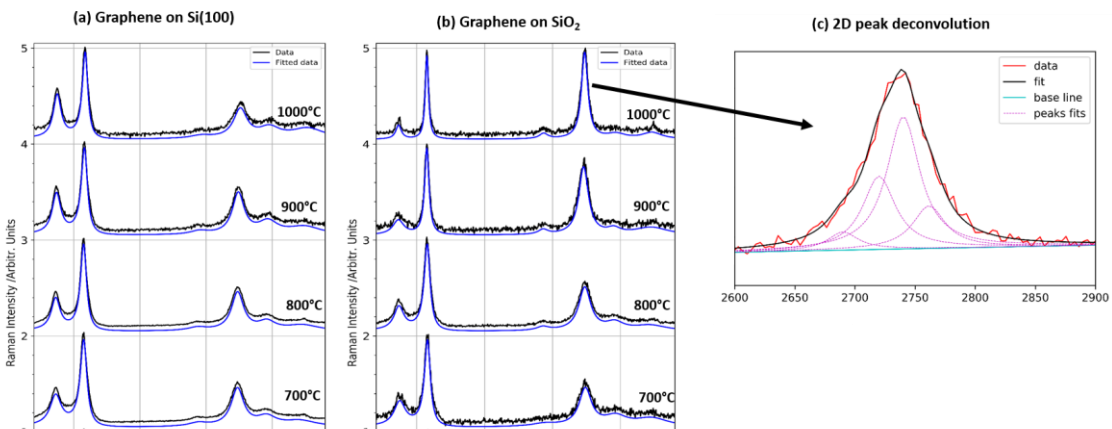

Fig. 4: Typical experimental (black) and fitted (blue) Raman spectra of graphene films grown at temperatures ranging from 600-1000°C: (a) on Si (100), (b) on SiO_2 (the red insert corresponds to the deconvolution of 2D peak of the spectrum of graphene at 1000°C on SiO_2).

3.2. Identification of nickel silicide phases when using Si(100) substrates

To understand the rather different impacts of increasing the annealing temperature on the growth of graphene when using Si(100) or SiO_2 substrates, the reactivity of the Ni catalyst layer with the substrate can be studied. Indeed, diffusion of Ni atoms into Si[33] and SiC[63,64] substrates during annealing, and the concomitant formation of nickel silicide phases have already been reported. This can influence the carbon diffusion process through the Ni catalyst as well as the nature of the resulting graphene film (number of layers, defects, etc.). In this study, the nickel silicide formation using Si(100) substrate was studied by Raman spectroscopy in the 100 to 500 cm^{-1} shift range, with a laser excitation at 633 nm, as shown in **Fig. 5**. The G-Si-600 sample (annealed at 600°C) exhibited no Raman peaks in this spectral region, suggesting that no nickel silicide is present. This could explain the small number of defects in the sample compared with the other samples synthesized at higher temperatures. In addition, the I_D/I_G mean ratio (0.297) of the G-Si-600 sample was quite close to the one (0.293) of G-SiO_2-600 (as other Raman characteristics, **Table 2**), also annealed at 600°C, suggesting that at this rather low temperature, both graphene films are very similar whatever the nature of the substrate.

At higher annealing temperatures, the evolution of the Raman response differed greatly in the two substrates, which can be correlated with the formation of nickel silicide on the Si(100) substrate. According to Raman spectral data in the literature[65–69], Ni_2Si, NiSi and $NiSi_2$ nickel silicide phases exhibit peaks at 100 and 140 cm^{-1}, 190 and 215 cm^{-1} and 230, 295, 320, and 370 cm^{-1}, respectively. In the present study, low wavenumber peaks related to Ni_2Si were

never observed whatever the annealing temperature. Bhaskaran *et al.*[69] observed significant background noise in the spectra in this region, and concluded that the presence of the Ni_2Si phase, formed by thermal processing of a Ni thin film on a silicon substrate, could not be confirmed.

A peak near 120 cm^{-1} (within the 117 and 123 cm^{-1} range) was observed at all temperatures, except surprisingly at 700°C. Huong et al.[70] attributed the 120 cm^{-1} peak to cylindrical graphene walls, but it was not possible to confirm their attribution here.

At 700°C, peaks corresponding to the formation of NiSi were observed, along with weak peaks probably associated with $NiSi_2$. Indeed, we cannot exclude the formation of a disilicide nickel phase, which is less Raman sensitive than the NiSi phase. At growth temperatures of 800°C and above, only the $NiSi_2$ Raman broad peaks were detectable at wavenumbers between 227 to 400 cm^{-1}, whereas the intense Raman signal of the NiSi phase decreased, which may be consistent with the transformation of the NiSi phase into the $NiSi_2$ phase at the highest temperatures (all Raman spectra were acquired with the same integration time). No similar phases were observed when the graphene was grown on the SiO_2 substrate, whatever the temperature (see **Supplementary S5**). The presence of nickel silicide phases is certainly responsible for the differences in the evolution of the Raman responses between the Si(100) and SiO_2 substrates, as highlighted in the following section.

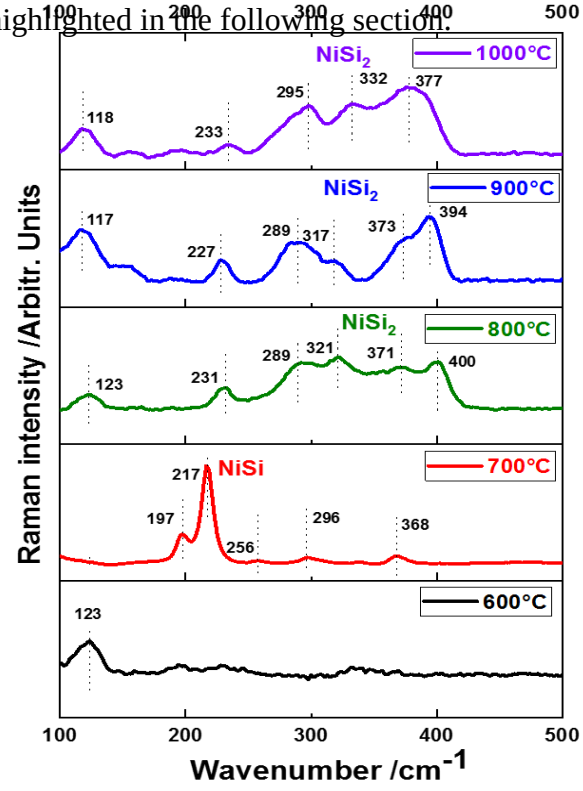

Fig. 5: Raman spectra at 633 nm for as-grown graphene on Si(100) with various growth temperatures from 600 to 1000°C. See text for peak assignments.

4. Discussion

4.1. Effect of the substrate on the graphene film nano-architecture

High quality few layer graphene is expected to exhibit low I_D/I_G and high I_{2D}/I_G ratios. From the Raman mapping of I_D/I_G and I_{2D}/I_G ratios, it appears that, for each substrate, graphene films with the lowest defects content and number of layers were G-Si-600 and G-SiO_2-1000. The G-Si-600 film exhibited I_D/I_G and I_{2D}/I_G ratios of 0.297 and 0.438 respectively, whereas the G-SiO_2-1000 film exhibited I_D/I_G and I_{2D}/I_G ratios of 0.140 and 0.721 respectively. In order to evaluate the dominant number of layers on the surface of the two samples compared with the literature, a statistical analysis of the number of graphene layers was performed by combining the I_{2D}/I_G and FWHM(2D) values deduced from the 400 spectra recorded on each sample. This analysis quantified the distribution of the I_{2D}/I_G and FWHM(2D) values between their minimum and maximum values for each graphene film. As can be seen in **Fig. 6**, I_{2D}/I_G varied from 0.40 to 0.46 and FWHM(2D) varied from 107 to 114 cm^{-1} in the G-Si-600 sample, whereas I_{2D}/I_G varied from 0.40 to 1.10 and FWHM(2D) varied from 20 to 90 cm^{-1} in the G-SiO_2-1000 sample. Based on **Table 1**, which correlates I_{2D}/I_G and FWHM(2D) with the number of layers in the samples from the 50 references in the literature, multilayered (>5) graphene is present on 100% of the G-Si-600 samples. In the G-SiO_2-1000 sample, 90% of the spectra present an I_{2D}/I_G ranging from 0.65 to 1.10, and a FWHM(2D) ranging from 50 to 80 cm^{-1}. The combination of both I_{2D}/I_G and FWHM(2D) indicates a predominant formation of 2–3 graphene layers on the SiO_2 substrate. Therefore, it can be concluded that the G-Si-600 sample has homogeneous architecture comprised of 100% of multilayered graphene, while the G-SiO_2-1000 sample predominantly exhibits a bi- and trilayer architecture.

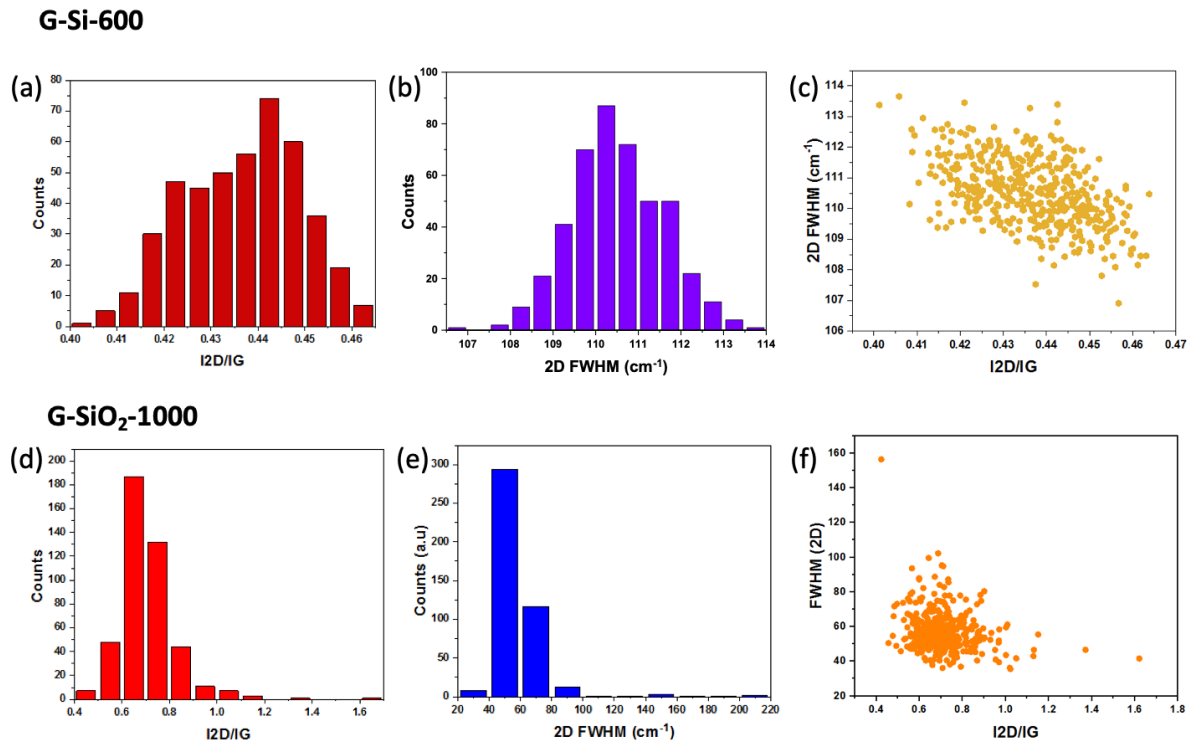

Fig. 6: (a) Histogram of the I_{2D}/I_G intensity ratio measured by Raman spectroscopy of 400 graphene films of the G-Si-600 sample, (b) Histogram of the FWHM(2D) peak measured by Raman spectroscopy for 400 graphene films of the G-Si-600 sample (c) FWHM(2D) peak plotted against the I_{2D}/I_G ratio for G-Si-600. (d) Histogram of the I_{2D}/I_G intensity ratio measured by Raman spectroscopy for 400 graphene films of the G-SiO_2-1000 sample. (b) Histogram of the FWHM(2D) peak measured by Raman spectroscopy for 400 graphene films of the G-SiO_2-1000 sample (c) FWHM(2D) peak plotted against the I_{2D}/I_G ratio for the G-SiO_2-1000 sample.

4.2. Differential effect of annealing temperature related to nickel silicide formation

In addition to Raman mappings of peak ratios and peaks FWHM, the D, G, and 2D peak positions were mapped (see **Supplementary S2, S3, S4**). Along with the study of I_{2D}/I_G and I_D/I_G, the evolution of those positions with annealing temperature is shown in **Fig. 7** for each substrate. In general, the G peak position follows the I_D/I_G ratio evolution, in good agreement with what was observed on graphite[71,72], with both values increasing with the nanoclustering and the reduction in crystallite size. However, one cannot exclude the impact of compressive stress leading to the G peak upshift, as already reported in other works[73–75]. This can be a concern especially in the case of nickel silicide formation leading to a surface texturing of the substrate during post-annealing cooling of the films. It is possible to correlate the increase or decrease in the 2D peak position with an opposite trend of the I_{2D}/I_G ratio. This is to be

expected when referring the literature, as the increase in the number of graphene layers upshifts the position of the 2D peak[74,76]. Here, the position of the D peak appears to behave in the same way as the position of the G peak and the I_D/I_G ratio, although it shifts almost twice as far as the G peak. Relatively few opinions have been expressed in the literature about the position of the D peak, but we suggest that the nanoclustering effects leading to the G peak upshift might produce the same outcome for the D peak.

When considering the SiO_2 substrate, increasing the annealing temperature has beneficial effects on the graphene quality. An increase in I_{2D}/I_G, a decrease of I_D/I_G and a decrease in the positions of the D, G, and 2D peaks indicate that the produced graphene has fewer layers (between 2 and 3) and fewer defects (higher homogeneity). Even though the process of graphene generation using a metal catalyst has not yet been fully elucidated, it appears that the phenomenon is enhanced when the annealing temperature is increased.

This is not the case when graphene is grown on Si substrate. The impact of temperature appears to be negligible, or at least comparable with what happens on SiO_2 up to 800°C. However, temperatures of 900°C and 1000°C are clearly detrimental to graphene quality, with I_{2D}/I_G decreasing and the other parameters increasing (I_D/I_G, D, G, and 2D positions). This means that in this case, the resulting material is a so-called multilayer graphene of a more defective nature. And, as can be seen in **Fig. 7**, these detrimental effects arise precisely when the most distinctive features of $NiSi_2$ are present in the Raman signature of the films.

It therefore appears that a high annealing temperature is beneficial for the quality of graphene grown using a nickel catalyst, except when the nickel reacts with the substrate. Indeed, the results for SiO_2 produced at high temperatures appear to originate in the optimal interaction of the a-C films with its Ni catalyst. It appears that when nickel silicides grow on the surface of Si substrates, less catalyst is available to produce graphene during annealing. If one considers that the Ni is consumed during graphene growth, increasing the temperature optimizes the consumption in the case of SiO_2, but not in the case of Si, as part of the Ni is consumed to produce nickel silicide. The formation of such nickel silicide phases reduces the proportion of the metallic nickel phase in which carbon may diffuse towards surface segregation of graphene. So, with Si(100), a higher proportion of carbon segregates at the surface, compared to what is observed with SiO_2 with no nickel silicide phase formation. Such a difference may explain why, with Si(100), the graphene film is thicker and multilayered, whereas with SiO_2 it is thinner with only 2-3 layers.

It has previously been suggested that the more defective nature of graphene samples grown on silicon using nickel as a catalyst is due to the nano-roughness induced by the formation of nickel silicide. The present work reveals that more complex phenomena may be involved here, in particular, the quantity of nickel available for both graphene growth and nickel silicide formation appears to be critical for the production of few-layer graphene.

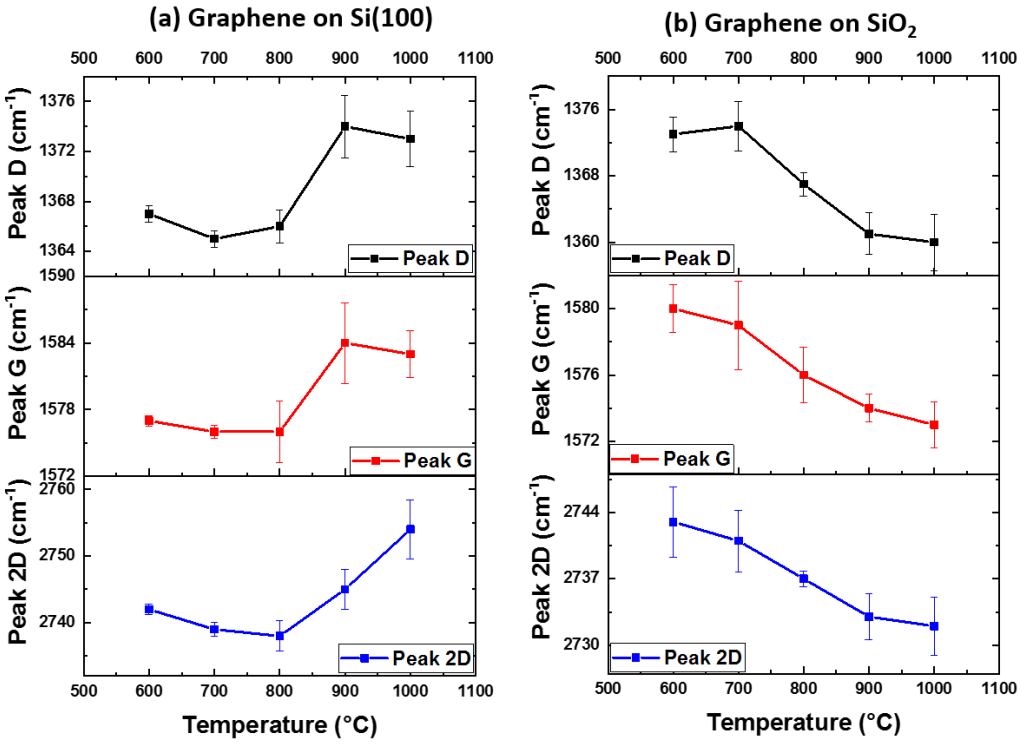

Fig. 7: D, G, and 2D peak positions depending on growth temperature for graphene grown on (a) Si(100), (b) on SiO_2.

5. Conclusions

In this paper, we report comparative Raman analysis of the graphene films prepared on Si(100) and SiO_2 substrates by combining high-vacuum pulsed laser deposition and rapid thermal annealing in low vacuum at growth temperatures ranging from 600 to 1000°C, in the presence of a Ni catalyst layer. The objective was to compare the nature of the graphene films grown from a similar amorphous carbon film, in similar thermal conditions but on two different substrates. The main conclusions are the following:

- A review of 50 literature references showed that the I_{2D}/I_G ratio and the FWHM of the 2D peak constitute Raman fingerprints that can be used to differentiate graphene nanoarchitectures with a number of layers ranging between 1 and 5, but with some uncertainties due to only partial recovery of these fingerprint ranges from one reference to another.
- The two different Si(100) and SiO_2 substrates, with an identical a-C/Ni top layer, are covered by a quite similar graphene film when growth occurs at 600°C. Growth at temperatures ranging from 700 to 1000°C induces very different behavior of the Raman signal, highlighting a significant effect of the substrate on the nanoarchitecture of the graphene film. The formation of nickel silicide phases between 700 and 1000°C, particularly above 900°C, is responsible for this difference.
- On the Si(100) substrate, increasing growth temperature leads to the synthesis of defective multilayered graphene film, with a decrease in the crystallite size with temperature.
- On the SiO_2 substrate, the increase in growth temperature results in a less defective graphene film, mainly comprised of 2-3 layers with larger crystallites.
- Higher annealing temperature benefits graphene growth when Ni is used as a catalyst on SiO_2, and this appears to be due to optimal consumption of the catalyst during the synthesis. This effect is cancelled during growth on Si, as the formation of nickel silicide, which increases at higher temperatures, limits the amount of catalyst available for graphene synthesis.

These findings underline the fact that, beyond parameters such as annealing temperature and synthesis conditions, the choice of an appropriate substrate for growth of graphene from a solid source using a metal catalyst is a useful tool to control the properties of graphene, including the number of defects and the number of layers.

Acknowledgements

This work was conducted with the financial support of the Future Program Lyon Saint-Etienne (PALSE) in the framework of the LABEX MANUTECH-SISE (ANR-10-LABX-0075) from the University of Lyon (ANR-11-IDEX-0007), under the *Investissements d'Avenir* program managed by the French National Research Agency (French acronym ANR).

References

[1] R. R. Nair, P. Blake, A. N. Grigorenko, K. S. Novoselov, T. J. Booth, T. Stauber, N. M. R. Peres, A. K. Geim, *Science* **2008**, *320*, 1308.
[2] C. Lee, X. Wei, J. W. Kysar, J. Hone, *Science* **2008**, *321*, 385.
[3] A. A. Balandin, S. Ghosh, W. Bao, I. Calizo, D. Teweldebrhan, F. Miao, C. N. Lau, *Nano Lett.* **2008**, *8*, 902.
[4] R. S. Edwards, K. S. Coleman, *Acc. Chem. Res.* **2013**, *46*, 23.
[5] K. I. Bolotin, K. J. Sikes, Z. Jiang, M. Klima, G. Fudenberg, J. Hone, P. Kim, H. L. Stormer, *Solid State Commun.* **2008**, *146*, 351.
[6] D. L. Nika, A. A. Balandin, *Rep. Prog. Phys.* **2017**, *80*, 036502.
[7] H. Malekpour, A. A. Balandin, *J. Raman Spectrosc.* **2018**, *49*, 106.
[8] K. S. Novoselov, V. I. Fal′ko, L. Colombo, P. R. Gellert, M. G. Schwab, K. Kim, *Nature* **2012**, *490*, 192.
[9] A. K. Geim, K. S. Novoselov, *Nat. Mater.* **2007**, *6*, 183.
[10] Y. D. Kim, M.-H. Bae, J.-T. Seo, Y. S. Kim, H. Kim, J. H. Lee, J. R. Ahn, S. W. Lee, S.-H. Chun, Y. D. Park, *ACS Nano* **2013**, *7*, 5850.
[11] F. Bonaccorso, Z. Sun, T. Hasan, A. C. Ferrari, *Nat. Photonics* **2010**, *4*, 611.
[12] T. Kuila, S. Bose, P. Khanra, A. K. Mishra, N. H. Kim, J. H. Lee, *Biosens. Bioelectron.* **2011**, *26*, 4637.
[13] J. Plutnar, M. Pumera, Z. Sofer, *J. Mater. Chem. C* **2018**, *6*, 6082.
[14] C. K. Chua, M. Pumera, *Chem Soc Rev* **2014**, *43*, 291.
[15] X. Ye, Q. Zhou, C. Jia, Z. Tang, Y. Zhu, Z. Wan, *Carbon* **2017**, *114*, 424.
[16] F. Liang, T. Watanabe, K. Hayashi, Y. Yao, W. Ma, Bin Yang, Y. Dai, *Mater. Lett.* **2017**, *187*, 32.
[17] M. Yi, Z. Shen, *J. Mater. Chem. A* **2015**, *3*, 11700.
[18] F. Zarotti, B. Gupta, F. Iacopi, A. Sgarlata, M. Tomellini, N. Motta, *Carbon* **2016**, *98*, 307.
[19] C. Faugeras, A. Nerrière, M. Potemski, A. Mahmood, E. Dujardin, C. Berger, W. A. de Heer, *Appl. Phys. Lett.* **2008**, *92*, 011914.
[20] J. H. Chu, J. Kwak, T.-Y. Kwon, S.-D. Park, H. Go, S. Y. Kim, K. Park, S. Kang, S.-Y. Kwon, *ACS Appl. Mater. Interfaces* **2012**, *4*, 1777.
[21] C. Maddi, F. Bourquard, V. Barnier, J. Avila, M.-C. Asensio, T. Tite, C. Donnet, F. Garrelie, *Sci. Rep.* **2018**, *8*, 3247.
[22] B. Shen, J. Ding, X. Yan, W. Feng, J. Li, Q. Xue, *Appl. Surf. Sci.* **2012**, *258*, 4523.
[23] S. An, G.-H. Lee, S. W. Jang, S. Hwang, S. H. Lim, S. Han, *Carbon* **2016**, *109*, 154.
[24] P. Fortgang, T. Tite, V. Barnier, N. Zehani, C. Maddi, F. Lagarde, A.-S. Loir, N. Jaffrezic-Renault, C. Donnet, F. Garrelie, C. Chaix, *ACS Appl. Mater. Interfaces* **2016**, *8*, 1424.
[25] M. Miyoshi, Y. Arima, T. Kubo, T. Egawa, *Appl. Phys. Lett.* **2017**, *110*, 013103.
[26] Y. Bleu, F. Bourquard, T. Tite, A.-S. Loir, C. Maddi, C. Donnet, F. Garrelie, *Front. Chem.* **2018**, *6*, 00572.
[27] Y. Hao, L. Wang, Y. Liu, H. Chen, X. Wang, C. Tan, S. Nie, J. W. Suk, T. Jiang, T. Liang, J. Xiao, W. Ye, C. R. Dean, B. I. Yakobson, K. F. McCarty, P. Kim, J. Hone, L. Colombo, R. S. Ruoff, *Nat. Nanotechnol.* **2016**, *11*, 426.
[28] K. Shen, H. Sun, J. Hu, J. Hu, Z. Liang, H. Li, Z. Zhu, Y. Huang, L. Kong, Y. Wang, Z. Jiang, H. Huang, J. W. Wells, F. Song, *J. Phys. Chem. C* **2018**, *122*, 21484.
[29] M. H. Oliveira, T. Schumann, F. Fromm, R. Koch, M. Ostler, M. Ramsteiner, T. Seyller, J. M. J. Lopes, H. Riechert, *Carbon* **2013**, *52*, 83.
[30] S. P. Cooil, F. Song, G. T. Williams, O. R. Roberts, D. P. Langstaff, B. Jørgensen, K. Høydalsvik, D. W. Breiby, E. Wahlström, D. A. Evans, J. W. Wells, *Carbon* **2012**, *50*, 5099.

[31] G. K. Hemani, W. G. Vandenberghe, B. Brennan, Y. J. Chabal, A. V. Walker, R. M. Wallace, M. Quevedo-Lopez, M. V. Fischetti, *Appl. Phys. Lett.* **2013**, *103*, 134102.
[32] A. T. T. Koh, Y. M. Foong, D. H. C. Chua, *Diam. Relat. Mater.* **2012**, *25*, 98.
[33] T. Tite, V. Barnier, C. Donnet, A. Loir, S. Reynaud, J. Michalon, F. Vocanson, F. Garrelie, *Thin Solid Films* **2016**, *604*, 74.
[34] M. Qian, Y. S. Zhou, Y. Gao, J. B. Park, T. Feng, S. M. Huang, Z. Sun, L. Jiang, Y. F. Lu, *Appl. Phys. Lett.* **2011**, *98*, 173108.
[35] I. Kumar, A. Khare, *Appl. Surf. Sci.* **2014**, *317*, 1004.
[36] P. Ren, E. Pu, D. Liu, Y. Wang, B. Xiang, X. Ren, *Mater. Lett.* **2017**, *204*, 65.
[37] A. E. M. Abd Elhamid, M. A. Hafez, A. M. Aboulfotouh, I. M. Azzouz, *J. Appl. Phys.* **2017**, *121*, 025303.
[38] R. S. Weatherup, B. C. Bayer, R. Blume, C. Baehtz, P. R. Kidambi, M. Fouquet, C. T. Wirth, R. Schlögl, S. Hofmann, *ChemPhysChem* **2012**, *13*, 2544.
[39] A. C. Ferrari, J. C. Meyer, V. Scardaci, C. Casiraghi, M. Lazzeri, F. Mauri, S. Piscanec, D. Jiang, K. S. Novoselov, S. Roth, A. K. Geim, *Phys. Rev. Lett.* **2006**, *97*, 187401.
[40] L. M. Malard, M. A. Pimenta, G. Dresselhaus, M. S. Dresselhaus, *Phys. Rep.* **2009**, *473*, 51.
[41] A. C. Ferrari, *Solid State Commun.* **2007**, *143*, 47.
[42] A. Das, S. Pisana, B. Chakraborty, S. Piscanec, S. K. Saha, U. V. Waghmare, K. S. Novoselov, H. R. Krishnamurthy, A. K. Geim, A. C. Ferrari, A. K. Sood, *Nat. Nanotechnol.* **2008**, *3*, 210.
[43] D. Graf, F. Molitor, K. Ensslin, C. Stampfer, A. Jungen, C. Hierold, L. Wirtz, *Eur. Phys. J. Spec. Top.* **2007**, *148*, 171.
[44] S. Chen, Q. Li, Q. Zhang, Y. Qu, H. Ji, R. S. Ruoff, W. Cai, *Nanotechnology* **2012**, *23*, 365701.
[45] A. C. Ferrari, D. M. Basko, *Nat. Nanotechnol.* **2013**, *8*, 235.
[46] J.-B. Wu, X. Zhang, M. Ijäs, W.-P. Han, X.-F. Qiao, X.-L. Li, D.-S. Jiang, A. C. Ferrari, P.-H. Tan, *Nat. Commun.* **2014**, *5*, 5309.
[47] M. S. Dresselhaus, A. Jorio, A. G. S. Filho, R. Saito, *Philos. Trans. R. Soc. Lond. Math. Phys. Eng. Sci.* **2010**, *368*, 5355.
[48] D. Teweldebrhan, A. A. Balandin, *Appl. Phys. Lett.* **2009**, *94*, 013101.
[49] H. Malekpour, P. Ramnani, S. Srinivasan, G. Balasubramanian, D. L. Nika, A. Mulchandani, R. K. Lake, A. A. Balandin, *Nanoscale* **2016**, *8*, 14608.
[50] S. Amini, J. Garay, G. Liu, A. A. Balandin, R. Abbaschian, *J. Appl. Phys.* **2010**, *108*, 094321.
[51] I. Calizo, W. Bao, F. Miao, C. N. Lau, A. A. Balandin, *Appl. Phys. Lett.* **2007**, *91*, 201904.
[52] I. Calizo, S. Ghosh, W. Bao, F. Miao, C. Ning Lau, A. A. Balandin, *Solid State Commun.* **2009**, *149*, 1132.
[53] G. Amato, F. Beccaria, E. Landini, E. Vittone, *J. Raman Spectrosc.* **2019**, *50*, 499.
[54] M. Bayle, N. Reckinger, A. Felten, P. Landois, O. Lancry, B. Dutertre, J.-F. Colomer, A.-A. Zahab, L. Henrard, J.-L. Sauvajol, M. Paillet, *J. Raman Spectrosc.* **2018**, *49*, 36.
[55] E. Cazzanelli, O. D. Luca, D. Vuono, A. Policicchio, M. Castriota, G. Desiderio, M. P. D. Santo, A. Aloise, A. Fasanella, T. Rugiero, R. G. Agostino, *J. Raman Spectrosc.* **2018**, *49*, 1006.
[56] M.-L. Lin, T. Chen, W. Lu, Q.-H. Tan, P. Zhao, H.-T. Wang, Y. Xu, P.-H. Tan, *J. Raman Spectrosc.* **2018**, *49*, 46.
[57] V. N. Popov, *J. Raman Spectrosc.* **2018**, *49*, 31.
[58] J. E. Weis, J. Vejpravova, T. Verhagen, Z. Melnikova, S. Costa, M. Kalbac, *J. Raman Spectrosc.* **2018**, *49*, 168.

[59] L. G. Cançado, K. Takai, T. Enoki, M. Endo, Y. A. Kim, H. Mizusaki, A. Jorio, L. N. Coelho, R. Magalhães-Paniago, M. A. Pimenta, *Appl. Phys. Lett.* **2006**, *88*, 163106.
[60] A. C. Ferrari, J. Robertson, *Philos. Trans. R. Soc. Lond. Ser. Math. Phys. Eng. Sci.*
[61] M. W. Iqbal, A. K. Singh, M. Z. Iqbal, J. Eom, *J. Phys. Condens. Matter* **2012**, *24*, 335301.
[62] F. Bourquard, Y. Bleu, A.-S. Loir, B. Caja-Munoz, J. Avila, M.-C. Asensio, G. Raimondi, M. Shokouhi, I. Rassas, C. Farre, C. Chaix, V. Barnier, N. Jaffrezic-Renault, F. Garrelie, C. Donnet, *Materials* **2019**, *12*, 666.
[63] E. Escobedo-Cousin, K. Vassilevski, T. Hopf, N. Wright, A. O'Neill, A. Horsfall, J. Goss, P. Cumpson, *J. Appl. Phys.* **2013**, *113*, 114309.
[64] Z.-Y. Juang, C.-Y. Wu, C.-W. Lo, W.-Y. Chen, C.-F. Huang, J.-C. Hwang, F.-R. Chen, K.-C. Leou, C.-H. Tsai, *Carbon* **2009**, *47*, 2026.
[65] S. Cichoň, P. Macháč, B. Barda, V. Machovič, P. Slepička, *Thin Solid Films* **2012**, *520*, 4378.
[66] F. F. Zhao, J. Z. Zheng, Z. X. Shen, T. Osipowicz, W. Z. Gao, L. H. Chan, *Microelectron. Eng.* **2004**, *71*, 104.
[67] P. S. Lee, *Electrochem. Solid-State Lett.* **1999**, *3*, 153.
[68] S. K. Donthu, D. Z. Chi, S. Tripathy, A. S. W. Wong, S. J. Chua, *Appl. Phys. A* **2004**, *79*, 637.
[69] M. Bhaskaran, S. Sriram, T. S. Perova, V. Ermakov, G. J. Thorogood, K. T. Short, A. S. Holland, *Micron* **2009**, *40*, 89.
[70] P. V. Huong, R. Cavagnat, P. M. Ajayan, O. Stephan, *Phys. Rev. B* **1995**, *51*, 10048.
[71] A. C. Ferrari, J. Robertson, *Phys. Rev. B* **2000**, *61*, 14095.
[72] A. C. Ferrari, J. Robertson, *Philos. Trans. R. Soc. Lond. Ser. Math. Phys. Eng. Sci.* **2004**, *362*, 2477.
[73] J. Röhrl, M. Hundhausen, K. V. Emtsev, Th. Seyller, R. Graupner, L. Ley, *Appl. Phys. Lett.* **2008**, *92*, 201918.
[74] D. S. Lee, C. Riedl, B. Krauss, K. von Klitzing, U. Starke, J. H. Smet, *Nano Lett.* **2008**, *8*, 4320.
[75] Z. H. Ni, H. M. Wang, Y. Ma, J. Kasim, Y. H. Wu, Z. X. Shen, *ACS Nano* **2008**, *2*, 1033.
[76] T. A. Nguyen, J.-U. Lee, D. Yoon, H. Cheong, *Sci. Rep.* **2014**, *4*, 4630.